

---

This is an electronic reprint of the original article.  
This reprint may differ from the original in pagination and typographic detail.

Aryanfar, Yashar; Assad, Mamdouh El Haj; Khosravi, Ali; Atiqure, Rahman S.M.; Sharma, Shubham; Alcaraz, Jorge Luis García; Alayi, Reza

## Energy, exergy and economic analysis of combined solar ORC-VCC power plant

*Published in:*  
International Journal of Low-Carbon Technologies

*DOI:*  
[10.1093/ijlct/ctab099](https://doi.org/10.1093/ijlct/ctab099)

Published: 01/01/2022

*Document Version*  
Publisher's PDF, also known as Version of record

*Published under the following license:*  
CC BY

*Please cite the original version:*  
Aryanfar, Y., Assad, M. E. H., Khosravi, A., Atiqure, R. S. M., Sharma, S., Alcaraz, J. L. G., & Alayi, R. (2022). Energy, exergy and economic analysis of combined solar ORC-VCC power plant. *International Journal of Low-Carbon Technologies*, 17, 196-205. <https://doi.org/10.1093/ijlct/ctab099>

---

This material is protected by copyright and other intellectual property rights, and duplication or sale of all or part of any of the repository collections is not permitted, except that material may be duplicated by you for your research use or educational purposes in electronic or print form. You must obtain permission for any other use. Electronic or print copies may not be offered, whether for sale or otherwise to anyone who is not an authorised user.

# Energy, exergy and economic analysis of combined solar ORC-VCC power plant

Yashar Aryanfar<sup>1</sup>, Mamdouh El Haj Assad<sup>2</sup>, Ali Khosravi<sup>3</sup>, Rahman S.M. Atique<sup>2</sup>, Shubham Sharma<sup>4</sup>, Jorge Luis García Alcaraz<sup>5</sup> and Reza Alayi<sup>6,\*</sup>

<sup>1</sup>Department of Electrical Engineering and Computers Sciences, Autonomous University of Ciudad Juárez, Ciudad Juárez 32310, Mexico; <sup>2</sup>Sustainable and Renewable Energy Engineering Department, University of Sharjah, Sharjah, UAE; <sup>3</sup>Mechanical Engineering Department, Aalto University, Espoo, Finland; <sup>4</sup>Department of Mechanical Engineering, IKG Punjab Technical University, Jalandhar-Kapurthala Road, Kapurthala, 144603, Punjab, India; <sup>5</sup>Department of Industrial Engineering and Manufacturing, Autonomous University of Ciudad Juárez, Ciudad Juárez, 32310, Mexico; <sup>6</sup>Department of Mechanics, Germe Branch, Islamic Azad University, Germe, Iran

## Abstract

A renewable energy source, especially solar energy, is one of the best alternatives for power generation in rural areas. Organic Rankine cycle (ORC) can be powered by a low-grade energy source, suitable for small-scale power production in rural areas. This study investigates the combined power generation and cooling system using the combination of ORC and vapor compression cycle (VCC), where ORC is powered by a parabolic trough solar collector. Thermodynamic and economic simulation of the system is conducted for four different working fluids, which are R245fa, R114, R600 and R142b. It can be concluded that the thermal efficiency of the power plant increases by using the combined ORC-VCC system. The effect of thermodynamic parameters such as turbine inlet temperature and pressure on the system performance is also discussed, and the optimal design values are provided. The results show that the power plant uses R245fa as the minimum exergy destruction rate. The study indicates that R114 gives minimum cost function (PCEU) for 137°C turbine inlet temperature while the minimum PCEU for R142b is obtained at a turbine inlet pressure of 2500 kPa. Finally, the study indicates that the inlet pressure of the turbine has a significant impact on the system cost and thermal efficiency.

**Keywords:** ORCVCCParabolic trough collectorOrganic fluidsThermal efficiency

\*Corresponding author:  
reza\_alayi@yahoo.com

Received 7 October 2021; revised 21 November 2021; accepted 8 December 2021

## 1 INTRODUCTION

One of the major global problems is climate change due to greenhouse gas emissions from power plants, the transportation sector and other industrial sectors [1]. The change rate of global warming can be decreased by decreasing the emission of these gases into the atmosphere, which is the solution for the worldwide warming problem [2]. Carbon dioxide (CO<sub>2</sub>) is the main contributor to global warming, which has resulted from the combustion process of fossil fuels used in transportation and power generation [3]. Renewable energy sources such as geothermal, biomass, hydropower, solar and wind power should be used to minimize

CO<sub>2</sub> emissions [4]. Another promising solution in recovering the waste energy can significantly help us meet the energy demands and decrease CO<sub>2</sub> emissions [5].

Different configurations of organic Rankine cycle (ORC) power plants powered by geothermal energy sources have been investigated using energy and exergy analysis [6], where the ORC condenser had the highest exergy destruction rate. Moreover, this study presented a comprehensive review of different types of geothermal ORC power plants used in hydrogen and freshwater production and electricity production. Another work [7] reviewed ORC powered by a geothermal energy source using energy and exergy analysis. Moreover, economic and life cycle studies were also presented to compare geothermal ORC with

International Journal of Low-Carbon Technologies 2022, 17, 196–205  
© The Author(s) 2022. Published by Oxford University Press.

This is an Open Access article distributed under the terms of the Creative Commons Attribution License (<http://creativecommons.org/licenses/by/4.0/>), which permits unrestricted reuse, distribution, and reproduction in any medium, provided the original work is properly cited.

<https://doi.org/10.1093/ijlct/ctab099> Advance Access publication 21 January 2022

commercial power plants. Finally, the work introduced the environmental impacts caused by using a geothermal energy source to power the ORC power plant. A novel combination of geothermal ORC and absorption chiller has been proposed [8] for electricity and cooling production. Energy, exergy and economic (3E) analyses were conducted for this novel system to determine its performance. The work also implemented the MOPSO algorithm to obtain the optimum electricity and cooling costs and the optimum exergy efficiency.

The purpose of the multigeneration concept is to produce electricity, heating and cooling [9]. Multigeneration systems are usually classified as cogeneration, where power and heat are made, and trigeneration, where cooling, heat and power (CHP) are produced [10]. Due to the low thermal efficiency (30–40%; [11]) of conventional power plants, it is recommended to use waste heat as a heat source of EnergyEnergy to enhance the system efficiency [12]. The use of multigeneration systems has been increased during the last years, which would positively support the global energy demand [13]. Using a multigeneration system could result in lower greenhouse gas emissions to meet the regulations set by developed and developing countries to reduce the global warming effect. Combining CHP with renewable energy sources could improve the system economics and decrease the consumption of fossil fuel and hence in environmental pollution [14]. The small-scale combined CHP and CCHP systems powered by renewable energy sources could improve off-grid areas' social and economic environment [15].

The investigation of large CHP systems has been given a lot of focus recently. Such methods include Stirling engines, reciprocating engines and the ORC power plant [16]. Bellos and Tzivanidis [17] analyzed a trigeneration system powered by solar EnergyEnergy to produce cooling, heat and electricity for the building, where they used 100 m<sup>2</sup> area of trough solar collector (PTC). They considered production of 20 kW for cooling and heat as the maximum examined values. They assumed 2500 hours yearly as the system's operating time, and they calculated the payback period as 8.5 years. Khosravi and Syri [18] investigated an absorption chiller powered by a geothermal energy source, combined with a desalination unit and solar thermal collector. The waste heat generated in the absorption system was used as an energy source for the desalination unit. This heat recovery significantly increased the coefficient of performance of the absorption cycle. Khalilzadeh and Hossein Nezhad [19] investigated waste heat in a trigeneration system using 12 wind turbines (7.5 MW each), where a modified ORC with feedwater heat, absorption chiller and heat exchangers was used. Chaiwat [20] proposed EnergyEnergy, exergy, economic and environmental analysis for a multigeneration system using ORC, single-effect absorption chiller and drying room. Based on their results, the energy efficiency was ~17.23%, and the exergy efficiency was 15.13%. Siddiqui *et al.* [21] proposed a renewable energy system combined with a biomass gasification system, for which they noticed that the overall efficiency of the integrated system remarkably improved.

On the other hand, due to the low thermal efficiency of the ORCs, researchers are intrigued to improve the efficiency by

analyzing different methods. The selection of working fluid is an important issue that is encountered when designing an ORC. Taking into account that the working fluid needs should have low global warming potential (GWP) and ozone depletion potential (ODP) according to the Paris Agreement on climate change [22]. Regan and Tao [23] studied different working fluids for solar ORC powered by solar EnergyEnergy. They found about 11 working fluids suitable for the power plant when the power plant was operating at solar collector low or medium temperature. Khosravi *et al.* [24] presented ORC powered with geothermal and solar EnergyEnergy, where they proposed an artificial intelligence model to investigate the influence of various parameters on the system performance. They examined different organic fluids for ORC and stated that R1234yf resulted in the best version of ORC. Pabon *et al.* [25] designed thermal energy storage incorporated with a two-phase mechanical pumped loop (TMPL) to cool a concentrating photovoltaic system. They investigated the TMPL system with the low global GWP refrigerants (R1234yf and R1234ze(E)), which showed similar performance compared to R134a. This was a promising conclusion to replace the new refrigerants as working fluids for thermodynamic systems. In another study, Pabon *et al.* [26] conducted an experimental investigation for an evaporator in a refrigeration system. They found out that R1234yf showed a similar dynamic behavior as compared to R134a.

The literature showed that a renewable multigeneration system could better utilize energy and better exergy efficiency. The main objective of this work is to investigate a novel small-scale ORC and vapor compression cycle (VCC) powered by PTC. The system can work for power generation and heating in winter and power generation and cooling in summer. This paper presents 3E analyses of combined solar ORC-VCC power plant. The combined power generation and cooling system using an ORC powered by solar energy source and a VCC is analyzed using thermodynamic and economic simulation for four different working fluids, which are R245fa, R114, R600 and R142b. The paper outline is organized as follows: Section 1 presents the literature review of previous works done on the paper topic; Section 2 presents the materials and methods that includes the thermodynamic model in Section 2.1 and the governing equations in Section 2.1.1; Section 3 demonstrates mathematically the exergy analysis of the combined power plant; Section 4 presents the economic analysis of the combined power plant based on the cost functions of all power plant components; Section 5 presents graphically the simulation results to see the effect of the most important parameters on the power plant performance; and Section 6 presents the major outcomes obtained in this paper. The outcomes of the present work are as follows:

- 3E for the solar ORC VCC combined power plant is proposed.
- Analysis is conducted for four different working fluids, which are R245fa, R114, R600 and R142b.
- Exergy destruction rates of all components are evaluated.
- The minimum exergy destruction rate for the proposed power plant is for R245fa as the working fluid.

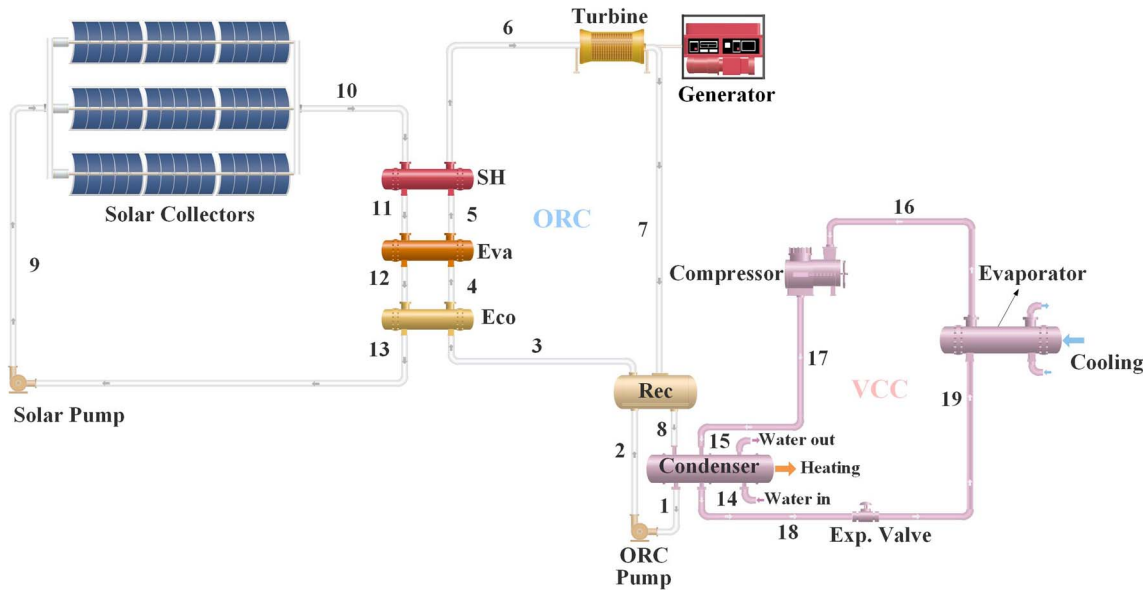


Figure 1. Combined power plant configuration.

- R114 results in minimum PCEU for 137°C turbine inlet temperature, and R142b results in minimum PCEU for 2500 kPa turbine inlet pressure.

## 2 MATERIAL AND METHODS

### 2.1 Thermodynamic modeling

The schematic diagram of the ORC-VCC is shown in Figure 1, and its T-S diagram is shown in Figure 2. The operating principles of ORC plants begin with the injection of an ORC fluid into the economizer, where it is heated to saturation temperature. The fluid state is modified from saturated liquid to saturated vapor in the evaporator, which operates at a constant temperature. The ORC fluid superconductor, the third heat exchanger, is superheated and raises the temperature at constant pressure. The superheated steam in state 6 reaches the turbine and generates electricity. The recuperator will reuse the turbine’s high steam energy output because of the turbine’s high steam energy output. The input is preheated before entering the economizer by the preheated infrared liquid recuperator. The recuperator fluid passes through the condenser, where it cools to the saturation liquid state. Finally, the economizer receives the working fluid.

#### 2.1.1 Governing equations

Mass balance. Mass balances are written as follows:

$$\dot{m}_1 = \dot{m}_8 + \dot{m}_{17} = \dot{m}_2 + \dot{m}_{18} \quad (1)$$

$$\dot{m}_2 = \dot{m}_3 = \dot{m}_4 = \dot{m}_5 = \dot{m}_6 = \dot{m}_7 \quad (2)$$

$$\dot{m}_9 = \dot{m}_{10} = \dot{m}_{11} = \dot{m}_{12} = \dot{m}_{13} \quad (3)$$

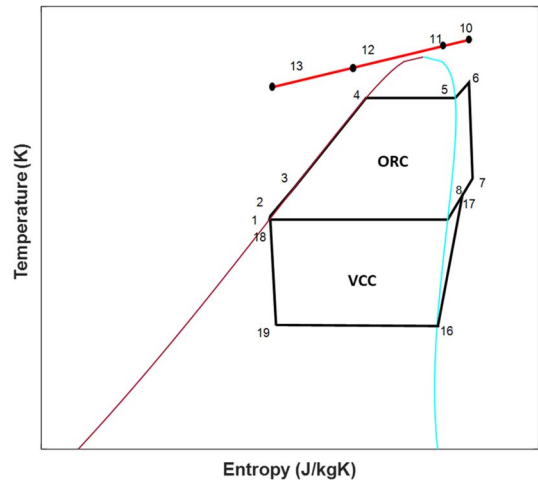


Figure 2. Temperature-entropy diagram.

$$\dot{m}_{16} = \dot{m}_{17} = \dot{m}_{18} = \dot{m}_{19} \quad (4)$$

$$\dot{m}_{14} = \dot{m}_{15} \quad (5)$$

ORC energy balance. The turbine isentropic efficiency is

$$\eta_t = \frac{\dot{W}_t}{\dot{W}_{t,s}} = \frac{h_6 - h_7}{h_6 - h_{7s}} \quad (6)$$

The turbine power output is

$$\dot{W}_t = \dot{m}_6 (h_6 - h_7), \quad (7)$$

where  $h$  is the specific enthalpy and the superscripted  $s$  refers to isentropic states.

The specific enthalpy of state 7 is obtained by calculating the isentropic vapor quality,  $x_{7s}$ , at the exit of the turbine as shown in the following equations:

$$x_{7s} = \frac{s_{7s} - s_{of}}{s_{fg}} \quad (8)$$

$$s_{7s} = s_6 \quad (9)$$

$$h_{7s} = h_f + x_{7s}h_{fg} \quad (10)$$

$$h_7 = h_6 - \eta_t (h_6 - h_{7s}), \quad (11)$$

where  $s$  is the specific entropy.

The condenser heat transfer rate is written as

$$\dot{Q}_C = (\dot{m}_8 + \dot{m}_{17}) h_{mix} - \dot{m}_1 h_1, \quad (12)$$

where  $h_1 = h_f(P_{cond})$  and  $h_{mix}$  are the specific enthalpy at the mixing point of states 8 and 17.

The equations used to calculate the pump power are

$$s_{2s} = s_1 \quad (13)$$

$$h_{2s} - h_1 = v_1 (P_2 - P_1) \quad (14)$$

$$\eta_p = \frac{h_{2s} - h_1}{h_2 - h_1}, \quad (15)$$

where  $\eta_p$  is the pump isentropic efficiency and  $v_1$  is the pump inlet specific volume. The pump work is then obtained as

$$\dot{W}_p = \dot{m}_1 (h_2 - h_1). \quad (16)$$

The power output is obtained by

$$\dot{W}_{net} = \dot{W}_t - \dot{W}_p. \quad (17)$$

The thermal efficiency is

$$\eta = \frac{\dot{W}_{net}}{\dot{Q}_{in}} \quad (18)$$

*Energy balance of VCC.* The cooling load in the evaporator is expressed as

$$\dot{Q}_{cool} = \dot{m}_{18} (h_{16} - h_{19}). \quad (18)$$

The required work by the compressor is written as

$$\dot{W}_{com} = \dot{m}_{16} (h_{17} - h_{16}). \quad (19)$$

The compressor isentropic efficiency is defined as

$$\eta_{is,com} = \frac{h_{17,s} - h_{16}}{h_{17} - h_{16}}, \quad (20)$$

which corresponds to the respective isentropic point.

The energy balance of the adiabatic expansion process in the throttling valve gives

$$h_{18} = h_{19}. \quad (21)$$

*Working fluids.* Four different working fluids, including R245fa, R114 and R142b refrigerants and R600 hydrocarbons, or n-butane, have been selected in this study. All these fluids are considered to be organic fluids. The specifications of these fluids are shown in Table 1. Among the most critical factors that influence fluid choice are GWP, ODP and atmospheric lifetime.

*Solar collector.* A parabolic PTC has been selected as a source of heat in this work. The radiation efficiency of the collector is 0.81 [19], and the intensity of the sunlight shown with  $G$  is also considered to be  $700 \text{ W/m}^2$  [20]. THERMINOL VP-1 is also used for the solar collector heat transfer oil [21]. The specifications of THERMINOL VP-1 are given in Table 2, where  $c_p$ ,  $\rho$  and  $k$  refer to the heat transfer fluid's specific heat, density and thermal conductivity, respectively.

### 3 EXERGY ANALYSIS

The concept of energy and exergy analysis is carried to find out the exergy destruction for the power plant.

The exergy destruction rates for the turbine, condenser, heat exchangers connecting the solar and ORC power plant, recuperator, evaporator, compressor and expansion valve are obtained, respectively, as follows

$$I_t = \dot{m}_{ORC} (h_6 - h_7 - T_0 * (s_6 - s_7)) - \dot{W}_t \quad (22)$$

$$I_{cond} = (Ex_{mix} + Ex_{14}) - (Ex_1 + Ex_{15}) \quad (23)$$

$$I_{pump} = \dot{m}_{ORC} (h_1 - h_2 - T_0 * (s_1 - s_2)) - \dot{W}_p \quad (24)$$

$$I_{HX} = (Ex_3 + Ex_{10}) - (Ex_6 + Ex_{13}) \quad (25)$$

$$I_{Rec} = (Ex_7 + Ex_2) - (Ex_8 + Ex_3) \quad (26)$$

$$I_{Evap,VCC} = (Ex_{19} + Ex_{hot\ air}) - (Ex_{16} + Ex_{cold\ air}) \quad (27)$$

$$I_{comp,VCC} = \dot{m}_{ORC} (h_{16} - h_{17} - T_0 * (s_{16} - s_{17})) - \dot{W}_{comp} \quad (28)$$

$$I_{val,VCC} = T_0 \dot{m}_{VCC} (s_{19} - s_{18}) \quad (29)$$

The overall exergy destruction rate of the combined cycle is

$$I_{tot} = I_t + I_{cond} + I_{pump} + I_{HX} + I_{Rec} + I_{Eva,VCC} + I_{comp,VCC} + I_{val,VCC}. \quad (30)$$

**Table 1.** Fluid properties.

Substance	Molecular mass (kg/mol)	T <sub>bp</sub> (°C)	T <sub>crit</sub> (°C)	P <sub>crit</sub> (MPa)	Atmospheric lifetime (yr)
R245fa	134.05	15.14	154	3.651	7.6
R114	170.92	3.6	145	3.289	300
R600	58.12	-0.5	152	3.796	0.018
R142b	100.5	-10	137	4.055	17.9

**Table 2.** Specifications of THERMINOL VP-1.

Fluid	T <sub>min</sub> /T <sub>max</sub> (°C)	ρ (kg/m <sup>3</sup> )	c <sub>p</sub> (kJ/kgK)	k (W/mK)
THERMINOL VP-1	12.78/398.9	1067.6	1.532	0.1368

**Table 3.** Capital cost functions.

Component	Capital cost function
Organic fluid turbine	4405 × (Ḡ <sub>tur</sub> ) <sup>0.89</sup>
Evaporator and condenser	1397 × (A <sub>eva or cond</sub> ) <sup>0.89</sup>
Heat exchanger	2143 × (A <sub>HE</sub> ) <sup>0.514</sup>
Pump	1120 × (Ḡ <sub>pump</sub> ) <sup>0.8</sup>
Recuperator	2681 × (A <sub>Rec</sub> ) <sup>0.59</sup>
Compressor	71.1 × $\frac{\dot{m} r_c}{0.01} \ln r_c$

## 4 ECONOMIC ANALYSIS

We also employed economic analysis besides energy and exergy analysis to determine the optimum operating condition for the system. Equation 31 calculates the system product cost rate (Ḡ<sub>tot</sub>) that is equal to the fuel cost rate (Ḡ<sub>fuel</sub>), the overall investment cost rate (Ḡ<sub>CI</sub>) and the rate of maintenance and operation cost (Ḡ<sub>OM</sub>) [27], which is written as

$$\dot{C}_{tot} = \dot{C}_{fuel} + \sum_k (\dot{Z}_{CI} + \dot{Z}_{OM})_k \quad (31)$$

and we have

$$\dot{Z}_{CI,k} + \dot{Z}_{OM,k} = \frac{Z_k \times \emptyset}{N \times 3600} CRF, \quad (32)$$

where N is the system annual working hours and CRF is the capital recovery factor, which is expressed by the following equation [28, 29]:

$$CRF = \frac{i(i+1)^n}{(i+1)^n - 1}, \quad (33)$$

where *i* and *n* are the annual effective rate and lifetime, respectively.

Table 3 summarizes the capital cost function for the power plant components

and for the solar collector:

$$Z_{coll} = 567 scroll, \quad (34)$$

where the collector surface area is

$$A_{coll} = \frac{\dot{Q}_{coll}}{\eta_{coll}G} \quad (35)$$

and the cost function is defined by

$$PCEU = \frac{C_{tot}}{[(\dot{W}_n + \dot{Q}_{eva}) \times n \times N]} \quad (36)$$

## 5 RESULTS AND DISCUSSION

### 5.1 Base mode analysis

The VCC cycle is off-grid in base mode, and the system only operates with the solar collector and the ORC cycle. Due to the superheater before the turbine, the fluid at the turbine inlet is superheated.

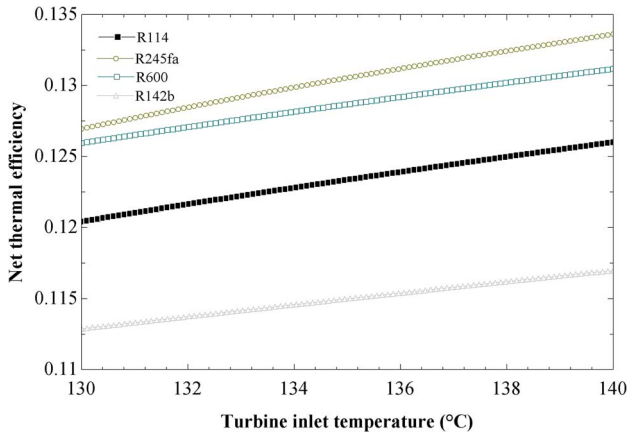
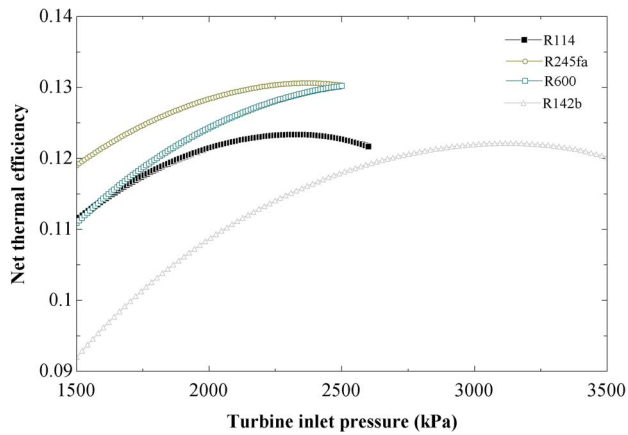
Figure 3 shows the effect of T<sub>6</sub> on the thermal efficiency (first-order efficiency) of the ground state system for the four studied fluids for fixed other parameters. As shown in Figure 3, the increase in T<sub>6</sub> results in the first law efficiency for all four fluids. As the temperature increases, the fluid energy content (or enthalpy) also increases, thereby increasing the system's thermal efficiency. This, of course, increases the difference between the solar collector's operating fluid inlet and outlet temperatures, and therefore requires a larger collector area, thus increasing the collector cost. As can be seen from Table 4, the highest thermal efficiency is related to the R245fa fluid, which is also illustrated in Figure 3. Generally, from a thermal efficiency point of view, increasing the T<sub>6</sub> has a positive effect on the energy performance of the base system.

Figure 4 presents the system thermal efficiency variation at the ground state relative to the turbine inlet pressure for the four studied fluids.

The figure shows an optimum pressure at which the thermal efficiency has a maximum value for all fluids. The reason for this behavior is due to the specific enthalpy of the operating fluid. When the output pressure of the turbine is constant and the inlet pressure increases, the specific enthalpy difference reaches a

**Table 4.** System output values for the base model.

	R142b	R600	R114	R245fa
$\eta$ (%)	11.51	12.87	12.34	13.06
$W_{\text{net}}$ (kW)	23.65	18.86	17.37	15.82
$\dot{m}_{\text{ORC}}$ (kg/s)	0.8931	0.3473	0.9385	0.5507

**Figure 3.** Variation of thermal efficiency with  $T_6$  in base mode.**Figure 4.** Variation of thermal efficiency with  $P_6$  in base mode.

maximum, which results in maximum thermal efficiency. Hence, the optimal system performance at the base state is at the pressure where the maximum thermal efficiency is reached.

The changes in the power output concerning the turbine inlet pressure are shown in Figure 5.

As shown in Figure 5, the total net output decreases as the turbine inlet pressure increases for three of the four fluids studied. Increasing the working pressure increases the power output of the turbine. However, the work required by the pump to produce the desired pressure also increases. On the other hand, increasing the mass flow rate reduces the ORC cycle performance. Therefore, the sum of these factors reduces the total output of the network for three fluids. But in the case of R142b fluid, the output work first increases and then decreases.

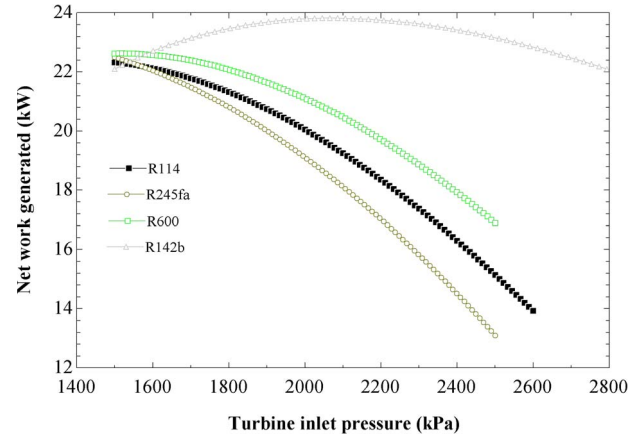
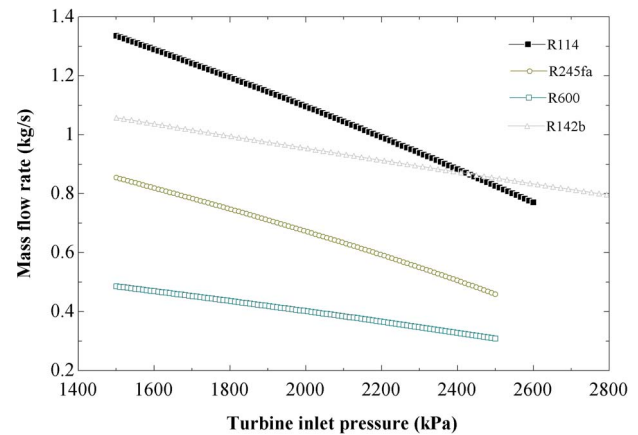
**Figure 5.** Variation of power output with  $P_6$  in base mode.**Figure 6.** Variation of organic fluid mass flow rate with  $P_6$  in base mode.

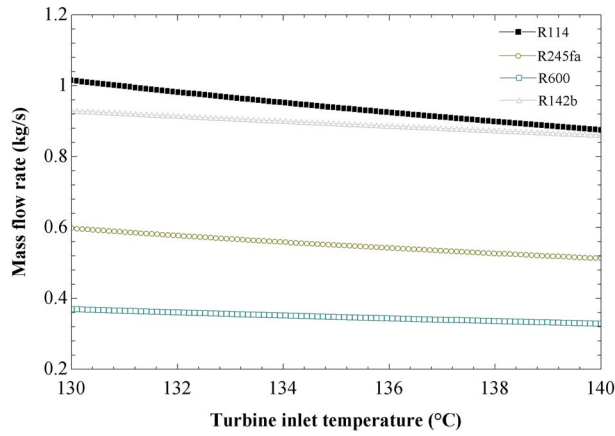
Figure 6 shows the effect of  $P_6$ , and Figure 7 shows the effect of  $T_6$  on the ORC power plant operating mass flow rate in the base state. As can be seen in both diagrams, the ORC mass flow rate decreases with increasing turbine inlet pressure and turbine inlet temperature. Reducing the mass flow reduces the amount of the total output of the network, which is an undesirable effect. But overall, it is a desirable factor for the system's operation, especially from the economic point of view of mass flow reduction. R600 fluid has the lowest mass flow rate, and the R114 fluid requires the highest mass flow rate for the system operation.

Figure 8 demonstrates the effect of  $T_6$  on the total grid output at the ground state for the four inorganic fluids.

As shown in the figure above, increasing  $T_6$  reduces the overall power output due to the reduction in the operating mass flow rate.

**Table 5.** System output values for ORC-VCC mode.

	R245fa	R142b	R600	R114
$\eta$ (%)	27.84	26.94	27.65	26.52
$W_{net}$ (kW)	12.94	23.92	17.02	15.02
$\dot{m}_{ORC}$ (kg/s)	0.419	0.818	0.288	0.755



**Figure 7.** Variation of organic fluid mass flow rate with  $T_6$  in base mode.

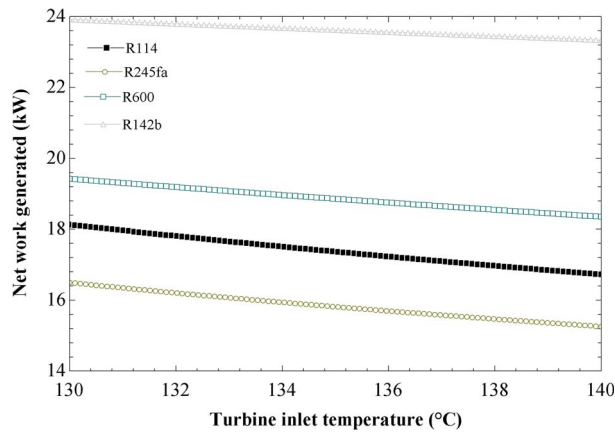


**Figure 8.** Power output versus  $T_6$  in base mode.

Increasing  $T_6$  improves the turbine's performance, but decreasing the mass flow rate reduces the amount of output work.

### 5.2 ORC-VCC mode analysis

The cases discussed in the previous section are also examined for the ORC-VCC mode. In the ORC-VCC mode, the VCC cycle switches from off-grid to on-grid, and this part of the system enters the network. For this simulation turbine, inlet pressure and temperature are 2500 kPa and 140°C, respectively. Table 5 summarizes the output values for the system in ORC-VCC mode.

As with the ORC cycle performance in the ground state, the fluid at the turbine inlet is superheated due to the presence of a superconductor before the turbine. Figures 9 and 10 show the

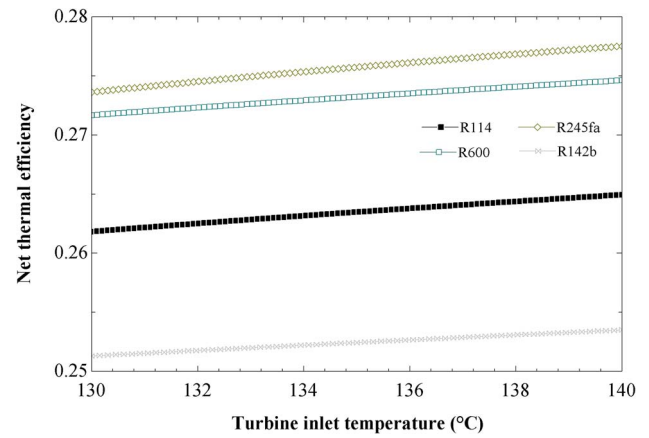


**Figure 9.** Variation of thermal efficiency with  $T_6$  in ORC-VCC mode.

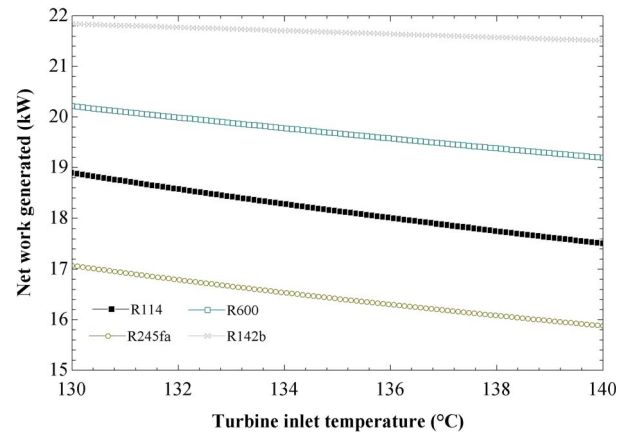


**Figure 10.** Power output versus  $T_6$  in ORC-VCC mode.

effect of  $T_6$  on the thermal efficiency of the system and net power generated in the ORC-VCC mode for the four fluids, respectively.

The increase in  $T_6$  improves the thermal efficiency and decreases the power output for all four fluids. In the basic model, the first law efficiency for the four fluids is in the range of 11–13.5%, while in the ORC-VCC mode, it is in the field of 25–26.5%, indicating a nearly two-fold increase in thermal efficiency.

Thermal efficiency variation with  $P_6$  for the four fluids is shown in Figure 11. As  $P_6$  increases, the thermal efficiency increases, reaching a maximum point, and then decreases. The highest possible thermal efficiency in ORC-VCC mode is for the operating fluid the R245fa when all the parameters are kept constant and only the turbine inlet pressure changes. The maximum thermal efficiency occurs at ~2500 kPa for R245fa.

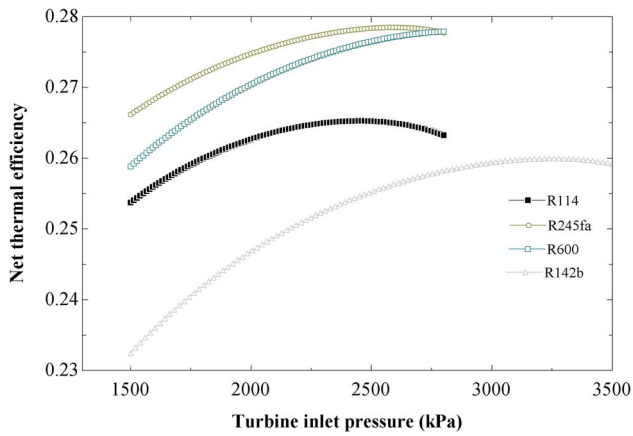


Figure 11. Thermal efficiency versus  $P_6$  in ORC-VCC mode.

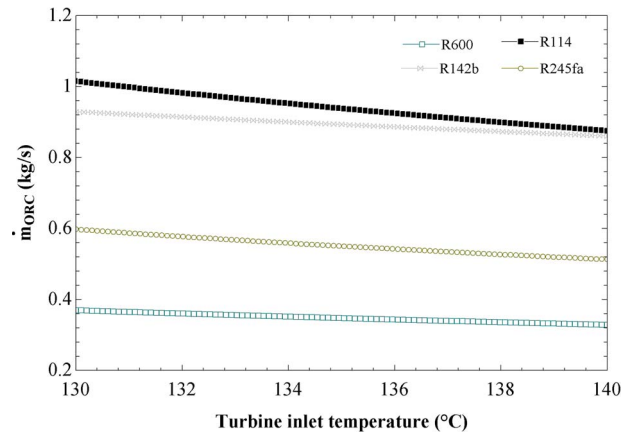


Figure 14. Variation of organic fluid mass flow rate with  $T_6$  in ORC-VCC mode.

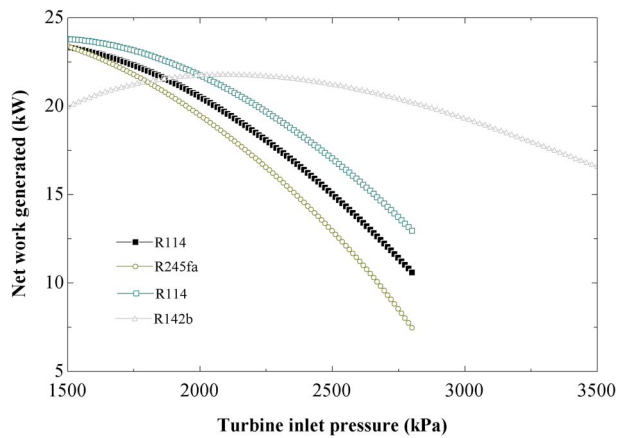


Figure 12. Variation of power output with  $P_6$  in ORC-VCC mode.

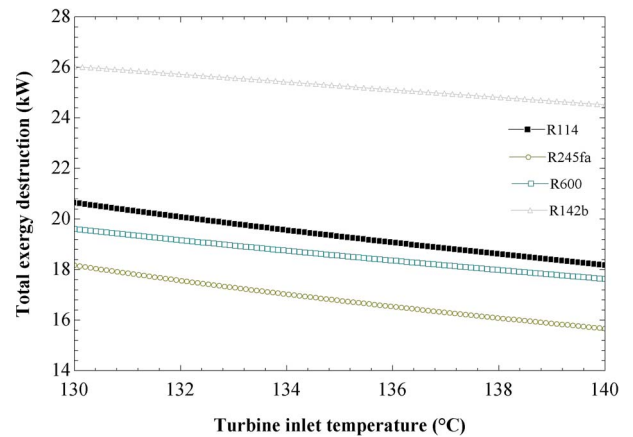


Figure 15. Effect of  $T_6$  on the total exergy destruction rate.

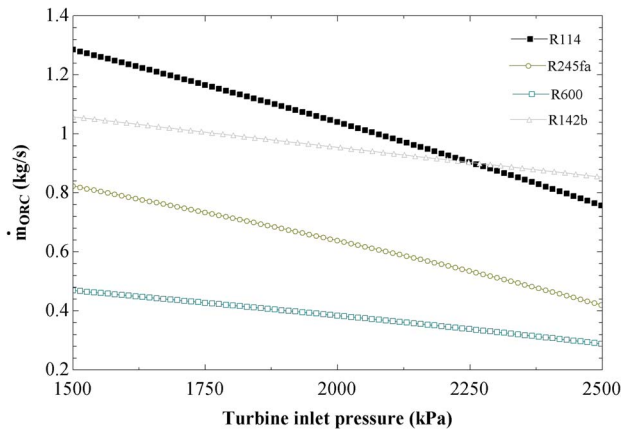


Figure 13. Variation of organic fluid mass flow rate with  $P_6$  in ORC-VCC mode.

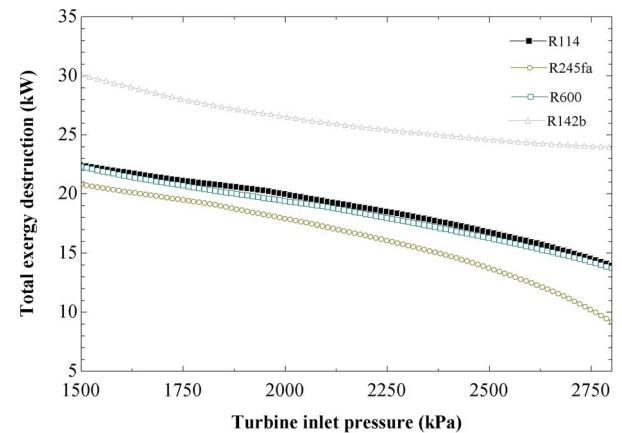


Figure 16. Effect of  $P_6$  on the total exergy destruction rate.

The changes in the power output of the combined power plant concerning the inlet pressure of the turbine for the four fluids in the ORC-VCC system are shown in Figure 12.

Figure 12 shows two different behaviors of the studied fluids as the turbine inlet pressure increases. For R245fa, R114 and R600 fluids, increasing  $P_6$  causes a decrease in the total output

of the grid output. But for R142b fluid, the whole workload of the network output first increases to a maximum point and then decreases. If all other parameters are assumed to be constant, and the system has the most efficient work, R600 fluid inlet pressure is the best option up to 2000 kPa and R142b is preferable for

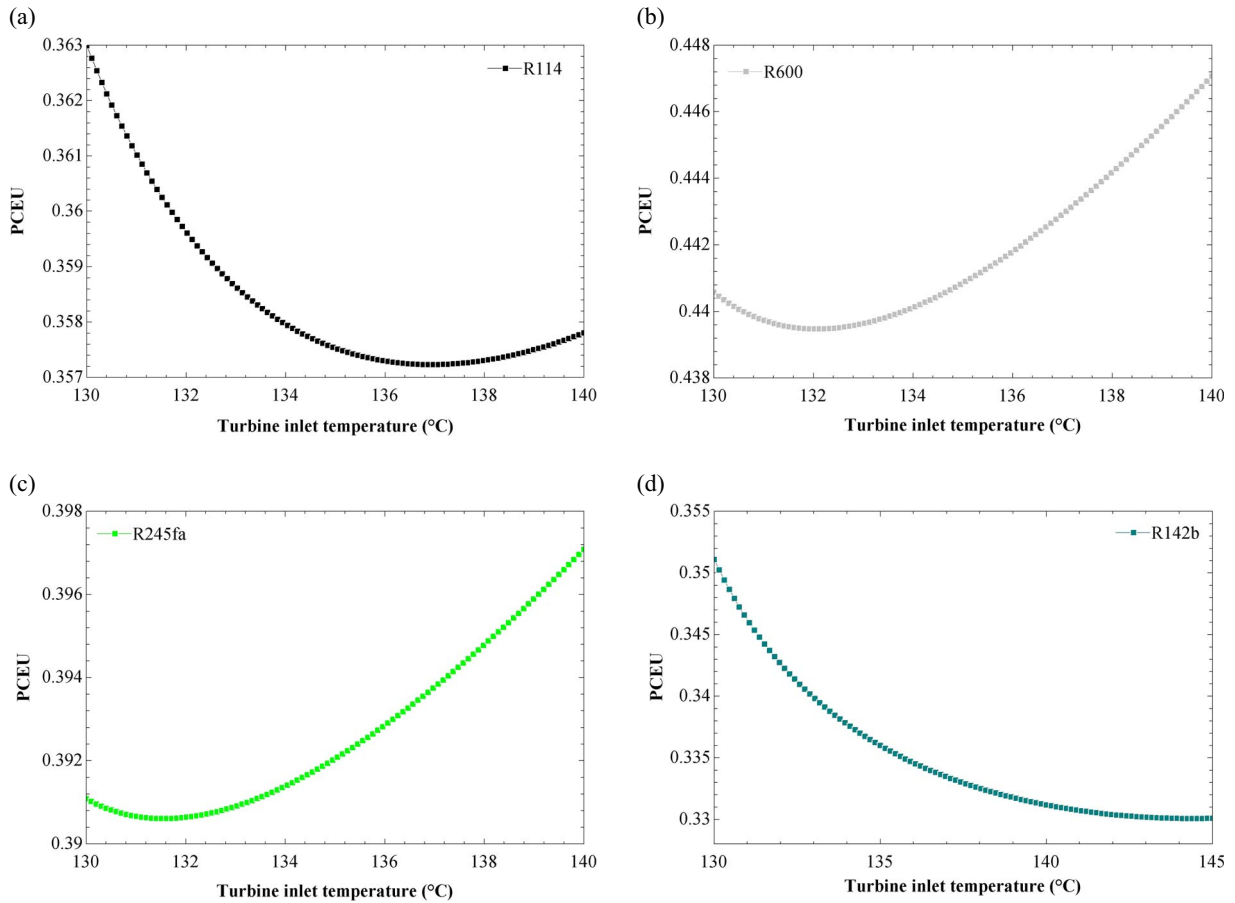


Figure 17. Effect of  $T_6$  on PCEU for different fluids.

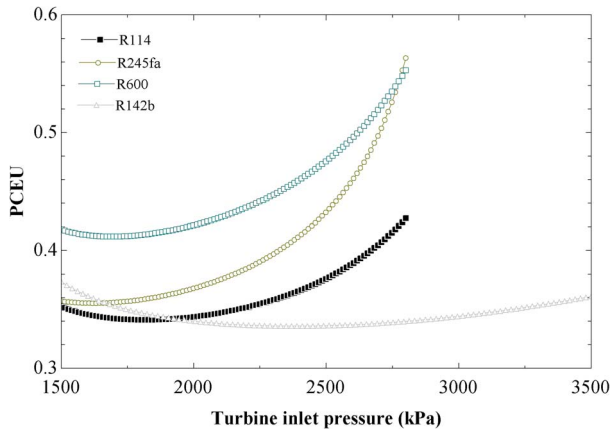


Figure 18. Effect of  $P_6$  on PCEU for different fluids.

higher fluid pressures. The total output of the network output in ORC-VCC mode is lower than in the basic mode.

Figure 13 shows the effect of  $P_6$ , and Figure 14 shows the effect of  $T_6$  on the four fluids' mass flow rate in ORC-VCC mode. The figures show that the ORC fluid mass flow rate decreases with increasing turbine inlet pressure and turbine inlet temperature.

By reducing the operating fluid mass flow rate, two important system outputs, namely the whole network operation and the heat absorbed by the evaporator, will be reduced. Therefore, when these two parameters are more important than the efficiency and economic aspects of the system, mass flow reduction is considered a negative change.

### 5.3 Exergy analysis

Figure 15 illustrates the effect of  $T_6$  over total exergy destruction for different working fluids. As can be seen from the figure, increasing the turbine inlet temperature decreases the total exergy destruction of the system. The system with R142b possesses the highest exergy destruction while the minimum exergy destruction belongs to R245fa. Figure 16 also shows the same behavior for turbine inlet pressure.

### 5.4 Economic analysis

Figure 17 demonstrates the effect of increasing the turbine inlet temperature over PCEU for each working fluid separately. The system working with R114 has the minimum PCEU when the turbine inlet temperature is  $\sim 137^\circ\text{C}$ . This figure also shows the

minimum PCEU for the system working with R600, R245fa and R142b achieved with the turbine inlet temperature of 132°C, 132°C and 145°C, respectively. Figure 18 illustrates the influence of turbine inlet pressure on PCEU. The results show that for R114, R245fa and R600, the optimum turbine inlet pressure is between 1500 and 2000 kPa. The minimum PCEU for R142b is obtained for the turbine inlet pressure of 2500 kPa.

## 6 CONCLUSIONS

Thermodynamic and economic analysis of an ORC power plant with PTC for small-scale power generation was investigated from 3E points of view. This research aimed to improve the thermal efficiency of the power generation system by using waste heat from the ORC to power the VCC cycle for cooling. Four fluids, namely R245fa, R114, R600 and R142b, were considered the operating organic fluids in this study. The VCC cycle utilized part of the dissipative heat in the condenser, which was used to cool the air to a temperature of 9°C. Using the VCC cycle simultaneously with the ORC cycle resulted in an increase in the system's thermal efficiency for all fluids by more than 100%. The effects of temperature and pressure at the turbine inlet on thermal efficiency and mass flow rate were investigated. According to the findings, an optimum input turbine pressure exists, which leads to maximizing thermal efficiency. The presence of a recuperator was critical because it improved thermal efficiency due to the heat recovery from the turbine outlet and the reduction of the loads on the condenser and solar collectors. The cycle with recuperator and superheater was the best schematic, but it had a higher overall cost.

The system working with R114 had the minimum PCEU when the turbine inlet temperature was ~137°C, whereas the minimum PCEU for R142b was obtained for the turbine inlet pressure of 2500 kPa. Finally, the parametric study indicated that turbine inlet pressure significantly impacts the system's thermal efficiency and overall cost.

## REFERENCES

- [1] US EPA. Climate Change Indicators: Greenhouse Gases.
- [2] Scientific American. 10 Solutions for Climate Change. <https://www.scientificamerican.com/article/10-solutions-for-climate-change/> (27 April 2021, date last accessed).
- [3] US EPA. Overview of Greenhouse Gases.
- [4] Malekan M, Khosravi A, Assad MEH. 2021. Parabolic trough solar collectors. In *Design and Performance Optimization of Renewable Energy Systems*. Elsevier.
- [5] Brückner S, Liu S, Miró L *et al*. Industrial waste heat recovery technologies: an economic analysis of heat transformation technologies. *Appl Energy* 2015;**151**:157–67.
- [6] Haghighi A, Pakatchian M, El-Haj Assad M *et al*. A review on geothermal organic Rankine cycles: modeling and optimization. *J Therm Anal Calorim* 2021;**144**:1799–814.
- [7] Ahmadi A, El-Haj Assad M, Jamali DH *et al*. Applications of geothermal organic Rankine cycle for electricity production. *J Clean Prod* 2020;**274**:122950.
- [8] Ehyaei MA, Ahmadi A, El-Haj Assad M, Rosen MA. Investigation of an integrated system combining an organic Rankine cycle and absorption chiller driven by geothermal energy: energy, exergy, and economic analyses and optimization. *J Clean Prod* 2020;**258**:120780.
- [9] Leiva-Illanes R, Escobar R, Cardemil JM *et al*. Exergy cost assessment of CSP driven multigeneration schemes: integrating seawater desalination, refrigeration, and process heat plants. *Energy Convers Manag* 2019;**179**:249–69.
- [10] Wang J, Wang J, Zhao P, Dai Y. Proposal and thermodynamic assessment of a new ammonia-water based combined heating and power (CHP) system. *Energy Convers Manag* 2019;**184**:277–89.
- [11] Karellas S, Braimakis K. Energy-exergy analysis and economic investigation of a cogeneration and trigeneration ORC-VCC hybrid system utilizing biomass fuel and solar power. *Energy Convers Manag* 2016;**107**:103–13.
- [12] Ashouri M, Razi Astarai F, Ghasempour R *et al*. Thermodynamic and economic evaluation of a small-scale organic Rankine cycle integrated with a concentrating solar collector. *Low Carbon Technol* 2015;**12**:ctv025.
- [13] Wang J, Yan Z, Wang M *et al*. Multi-objective optimization of an organic Rankine cycle (ORC) for low grade waste heat recovery using evolutionary algorithm. *Energy Convers Manag* 2013;**71**:146–58.
- [14] Al-Sulaiman FA, Dincer I, Hamdullahpur F. Exergy modeling of a new solar-driven trigeneration system. *Sol Energy* 2011;**85**:2228–43.
- [15] Al-Sulaiman FA, Dincer I, Hamdullahpur F. Thermoeconomic optimization of three trigeneration systems using organic Rankine cycles: Part II - applications. *Energy Convers Manag* 2013;**69**:209–16.
- [16] Ahmadi P, Dincer I, Rosen MA. Exergo-environmental analysis of an integrated organic Rankine cycle for trigeneration. *Energy Convers Manag* 2012;**64**:447–53.
- [17] Bellos E, Tzivanidis C. Parametric analysis of a solar-driven trigeneration system with an organic Rankine cycle and a vapor compression cycle. *Energy Built Environ* 2021.
- [18] Khosravi A, Syri S. Modeling of geothermal power system equipped with absorption refrigeration and solar energy using multilayer perceptron neural network optimized with imperialist competitive algorithm. *J Clean Prod* 2020;**276**.
- [19] Khalilzadeh S, Hossein Nezhad A. Using waste heat of high capacity wind turbines in a novel combined heating, cooling, and power system. *J Clean Prod* 2020;**276**:123221.
- [20] Chaiyat N. A multigeneration system of combined cooling, heating, and power (CCHP) for low-temperature geothermal system by using air cooling. *Therm Sci Eng Prog* 2021;**21**:100786.
- [21] Siddiqui O, Dincer I, Yilbas BS. Development of a novel renewable energy system integrated with biomass gasification combined cycle for cleaner production purposes. *J Clean Prod* 2019;**241**.
- [22] UNFCCC. The Paris Agreement. <https://unfccc.int/process-and-meetings/the-paris-agreement/the-paris-agreement> (12 April 2021).
- [23] Rayegan R, Tao YX. A procedure to select working fluids for solar organic Rankine cycles (ORCs). *Renew Energy* 2011;**36**:659–70.
- [24] Khosravi A, Syri S, Zhao X, Assad MEH. An artificial intelligence approach for thermodynamic modeling of geothermal based-organic Rankine cycle equipped with solar system. *Geothermics* 2019;**80**:138–54.
- [25] Pabon JGG, Khosravi A, Malekan M, Sandoval OR. Modeling and energy analysis of a linear concentrating photovoltaic system cooled by two-phase mechanical pumped loop system. *Renew Energy* 2020;**157**:273–89.
- [26] Garcia J, Ali T, Duarte WM *et al*. Comparison of transient response of an evaporator model for water refrigeration system working with R1234yf as a drop-in replacement for R134a. *Int J Refrig* 2018;**91**:211–22.
- [27] Selbaş R, Kizilkcan Ö, Şencan A. Thermoeconomic optimization of sub-cooled and superheated vapor compression refrigeration cycle. *Energy (Oxf)* 2006;**31**:2108–28.
- [28] Khosravi A, Koury RNN, Machado L. Thermo-economic analysis and sizing of the components of an ejector expansion refrigeration system. *Int J Refrig* 2017.
- [29] El Haj Assad, Aryanfar Y, Javaherian A *et al*. SMS Mahmoudi, energy, exergy, economic and exergoenvironmental analyses of transcritical CO<sub>2</sub> cycle powered by single flash geothermal power plant. *Int J Low-Carbon Technol* 2021;ctab076. <https://doi.org/10.1093/ijlct/ctab076>.